Radiation distributions in TCV

G. Veres [a,*] R.A. Pitts [b] M. Wischmeier [c] S. Kálvin [a]
B. Gulejova [b] J. Horacek [b]

[a] *KFKI-RMKI, EURATOM-Association, Budapest, Hungary*

[b] *CRPP-EPFL, Association EURATOM-Confédération Suisse, CH-1015 Lausanne, Switzerland*

[c] *Max-Planck-Institut für Plasmaphysik, EURATOM-Association, Boltzmann Str. 2., D-85748, Garching, Germany*

Abstract

Tomographically reconstructed total radiative powers from bolometer and AXUV camera systems are compared to SOLPS5 simulations in low and high density deuterium and helium diverted discharges on the TCV tokamak. For low density the match between simulation and measurements is satisfactory, but at high density strongly radiating regions outside the SOLPS5 simulation grid are seen in measurements and maybe due to enhanced convective particle transport in the low field side midplane region. The chord coverage of the foil bolometer system does not, however, allow detailed resolution in this region. The comparison of foil and AXUV data also demonstrates that ageing of the AXUV diodes under plasma irradiation combined with the unevenness of the diode spectral response, strongly limits their application for total radiative power measurements.

Key words: Divertor plasma, Impurity sources, Power balance, Radiation, TCV
PACS: 52.25, 52.40, 52.70

1 Introduction

Measurement of total radiation from tokamak plasmas is traditionally accomplished using tomographic inversion of the signals from bolometric cameras

* KFKI-Research Institute for Particle and Nuclear Physics, POB.49, H-1525, Budapest, Hungary
Email address: veres@rmki.kfki.hu (G. Veres).

[1]. Such systems are sensitive to radiation from both photonic and from neutral particles. They are relatively slow, with time constants in the millisecond range and can be difficult to interpret in some circumstances, particularly in X-point configurations at high density, when neutral densities are high and the basic assumption of tomography (that the plasma be transparent to all the measured radiation) cannot always be satisfied. An alternative technique is to employ linear photodiode arrays which have recently seen increasing use ([2–4]). These have the advantage of being considerably faster than foil bolometers (rise times in the μs range) and are insensitive to neutrals. However, such diodes have a thin (typically 3-7 nm SiO_2) surface passivation layer, acting as an entrance window and reducing spectral responsivity in the low energy region (few 10's eV, see Fig. 1) where a significant fraction of radiation - especially in the edge/SOL and divertors of carbon dominated machines such as TCV where much of the radiation originates [5]. In addition to this variable spectral response, AXUV diodes have another difficulty when in operation over many years on a tokamak: the surface passivation layer thickness increases under plasma light irradiation, resulting in a further decrease of their responsivity in precisely the same spectral range where the response is already reduced. To overcome this obstacle, regular calibration against a standard light source would be required in the 10-100 eV range (where no commonly available sources exist) or the diodes must be replaced at regular intervals. Alternatively, "radiation hardened" diodes can be used (the TCV diodes are the standard AXUV EL detectors available from IRD [6]), but these are not readily available in compact, multi-detector form, as required for tomographic purposes.

Accounting for the variable AXUV spectral response plus the ageing effect in TCV (where much of the radiation in most cases of interest originates from low ionisation states of carbon at low energies) is not possible without a complete model for the impurity production and transport. A primarily experimental comparison has thus been attempted, using low and high density ohmic plasmas in divertor configurations with deuterium and pure helium fuel species.

Helium plasmas have the attractive property of reduced charge-exchange neutral outfluxes and greatly reduced carbon concentrations, especially at high density, when a cold edge reduces physical sputtering of carbon in a regime in which carbon chemical sputtering is also largely absent (He is chemically inert and any chemical release is due to residual deuterium released from the walls). Helium has intense spectral lines in the same low energy range where carbon species radiate strongly, but the power released over those spectral lines is considerably lower for helium, than for carbon (see e.g. the ADAS database [7]). The influence on the total measured radiated power of the variable AXUV diode spectral response is therefore expected to be reduced in He plasmas with lower carbon concentrations.

2 Experimental setup

The TCV tokamak has been equipped for many years with a 5 camera, 64 channel foil bolometer diagnostic [8], covering the entire vessel cross-section at a single toroidal location. Recently, a new 7 camera, 140 chord AXUV system has been installed in a common sector toroidally displaced by 90° from the foil bolometers [9].

The results presented here were obtained in matched He and D single null lower, ohmic diverted plasmas (see Fig. 1) with plasma current of 340 kA. In addition to fuel species, the plasma density, $\bar{n}_e$ has also been varied either in the form of a density ramp up to values approaching the density limit in a single discharge ($\bar{n}_e \sim 3 \rightarrow 12 \times 10^{19}$ m^{-3} or in pulses with fixed density. The plasmas have $q_{95} \sim 3.5$ and triangularity, $\delta_{95} \sim 0.35$ for elongation $\kappa_{95} \sim 1.6$. Arrays of target embedded Langmuir probes are used to measure the power conducted and convected to the divertors and hence provide a check of overall power balance by comparison with total ohmic input and radiated power.

Tomographic reconstructions of foil bolometer and AXUV diode signals were obtained with first order linear regularization on a rectangular grid covering the whole plasma chamber [10]. Based on these images, both the spatial distributions of the radiative power and the time dependent total radiative power emitted by the plasma may be determined.

3 Results and Discussion

Figures 2a and 3a show, respectively, the time variation in low density D and He plasmas of the plasma effective charge estimated from the distribution of soft X-ray radiation measured by a separate tomographic array of cameras [10].

Following the establishment of the full divertor configuration (at around 0.43 s), $Z_{\text{eff}} \sim 1.2$ in D and about 2 in He, indicating low impurity concentrations in the plasma core. The time evolution of power balances for the two cases are illustrated in Figure 2b and 3b, where the ohmic input, is compared with the sum of the Langmuir probe (P_{SOL}) and radiative (P_{RAD}) powers. Extremely good balance is obtained ($P_\Omega = P_{SOL} + P_{RAD}$) only if the foil bolometer radiated power is assumed as the main radiative contribution - the AXUV system grossly underestimates the total.

Interestingly, the AXUV power time evolution qualitatively matches that of the Z_{eff} - a rather surprising result, suggesting that the AXUV diodes pick

up radiation mostly from the confined plasma region (from which the X-ray Z_{eff} is defined). These observation indicate at least two possible effects at play in determining the radiation fractions : the foil bolometry power (at least at low density) is negligibly influenced by any neutral contribution, and that the AXUV diodes (as a consequence of the reduced response at low energies and the ageing effect) are far too insensitive to the low energy edge radiation for them to be of use in estimating the total power.

Figures 4 and 5 show the power balances for the high density deuterium and helium discharges. In these cases clearly $P_\Omega < P_{SOL} + P_{RAD}$, which indicates that P_{RAD} is influenced by the neutral radiation. In the case of the deuterium discharge, the total foil bolometry radiated power is more than 50 % of the Ohmic input, whereas in the helium discharge P_{RAD} is only about 30 %of the Ohmic input at comparable AXUV (core radiation) powers.

The poloidal radiation distributions provided by the tomographic reconstruction provide an excellent experimental benchmark by which to test the results of edge code simulations of the TCV SOL. Such simulations have recently been performed using the SOLPS5 (B2.5-Eirene) code package [11] for He and D plasmas in precisely the discharge configuration used here [13,12].

To compare code with experiment, the measured total radiative powers have been integrated over three specific regions: *1* - the area corresponding exactly to that covered by the SOLPS5 simulation grid (comprising all flux surfaces located 3 cm inside the midplane separatrix to 1.8 cm beyond it into the SOL) *2* - the region not covered by SOLPS5 inside the separatrix, and *3* - the region not covered by SOLPS5 outside the separatrix. Figures 7-8 plot these three regions separated by flux surfaces shown by white lines.

A common feature of all Figures 7-9 is that the SOLPS5 simulation predicts higher radiation than derived from the foil bolometers around the top high field side of the plasma at all densities studied. The origin of this discrepancy can be traced to a temperature drop (in the code simulation) in the vicinity of the upper X-point (located outside the vacuum vessel in this configuration). The code assumes impurities to be evenly eroded from all plasma-facing surfaces and this, combined with the low temperatures and long residence times of low charge state ionised impurities near the second X-point, provides for the high predicted radiation. Such trends are evidently not observed experimentally - except a slight radiation increas in that reagion in the high density He discharge, Fig. 9 - , pointing to an inaccurate description of the impurity production in this region.

Whilst the code predicts a radiation source where none is found experimentally, the foil bolometry reconstructions clearly show enhanced radiation sources around the low field side (LFS) midplane region. Unfortunately the bolome-

ter chord coverage (there are no sight lines crossing the LFS main chamber wall other than those belonging to the cameras mounted on the outboard lateral ports (see Fig. 1) does not permit detailed resolution in this region. In the absence of sufficient crossed chords the tomography procedure will always 'concentrate' the radiation into the regions, i.e. at the top right and middle lateral cameras. However, the AXUV images also show a radiating zone on the LFS wall at the height of the magnetic axis, but in this case the reduced sensitivity prevents a detailed study. On possible explanation for these LFS radiation zones is an enhanced level of particle transport in the outboard midplane region. Such transport has recently been directly measured and quantified on TCV by comparing observations of the turbulent density and flux time series with predictions of a 2D fluid turbulence code [14]. Increased convective transport of this nature has in fact also been a necessary inclusion in the high density SOLPS5 simulations used here (see Figs 8, 9 and Table 1 cases #10841, #11150) in order to approach the levels of divertor detachment that are seen at the outer target at high density [12]. Such transport has potential for impurity release and should be more noticeable in D plasmas where the relatively low energy turbulent fluxes can more readily release C impurities through chemical sputtering. This appears to be the case when comparing the D and He reconstructions at high density in Figs 8 and 9.

Table 1. summarizes the total radiative power measured and simulated for the three regions for low/high densities and He/D plasma species. At low densities the SOLPS5 power is rather well matched by foil bolometry power, but there is a substantial power generated by radiation outside the region covered by the simulation grid. This provides strong motivation to attempt to extend the simulation grid to the wall shadow regions in the longer term. At high densities in contrast, only the sum of the bolometer radiation inside and outside the code simulation domain is close to the predicted power. This might indicate that either some of the power assumed by SOLPS5 to be generated inside its grid area in fact is generated outside, or that SOLPS5 simply overestimates the power radiated in the simulated region. In addition to the convective transport, the code simulation case #10841 was performed using an artificially enhanced *Ychem* at the main chamber wall of 10% in order to produce the observed levels of divertor detachment [13]. Moreover, the enhanced *Ychem* was assumed to be poloidally uniform. In the He case, the power accounting is improved, providing further evidence that the discrepancy at high density is linked to the way in which impurity release is simulated

Comparing the foil and AXUV bolometry derived total radiation, both are well matched at all densities and for both He and D only for the central, confined plasma region, but not elsewhere. This is direct further evidence for the combined effect of diode ageing and reduced response at low energies, demonstrating that the AXUV diagnostic can only offer quantitative measurements of radiation from the core regions.

References

[1] K. McCormick, A. Huber, C. Ingesson et al., *Fusion Eng. and Design* **74** (2005) 679.

[2] R.L. Boivin, J.A. Goetz, E.S. Marmar et al., *Rev. Sci. Instrum.* **70** (1999) 260.

[3] D.S. Gray, S.C. Luckhardt, L. Chousal et al., *Rev. Sci. Instrum.* **75** (2004) 376.

[4] C. Suzuki, B.J. Peterson, K. Ida, *Rev. Sci. Instrum.* **75** (2004) 4142.

[5] A.W. Leonard, M.A. Mahdavi, S.L. Allen et al., *Phys. Rew. Lett.* **78** (1997) 4769.

[6] http://www.ird-inc.com

[7] http://www-cfadc.phy.ornl.gov/adas/adas.html

[8] I. Furno, H. Weisen, J. Mlynar et al., *Rev. Sci. Instrum.* **70** (1999) 4552.

[9] A.W. Degeling, H. Weisen, A. Zabolotsky et al., *Rev. Sci. Instrum.* **75** (2004) 4139.

[10] M. Anton, H. Weisen, M.J. Dutch et al., *Plasma Phys. Contr. Fusion* **38** (1996) 1849.

[11] R. Schneider, X. Bonnin, K. Borrass et al., *Contrib. Plasma Phys.* **46** (2006) 3.

[12] M. Wischmeier, R.A. Pitts, J. Horacek et al., *32nd EPS Conference on Plasma Phys. Tarragona, 27 June - 1 July 2005* **ECA Vol.29C**, (2005) P-5.013.

[13] M. Wischmeier, Simulating divertor detachment in the TCV and JET tokamaks, *PhD thesis in CRPP report* **LRP 799/05** (2005).

[14] O.E. Garcia et al., *Plasma Phys. Contr. Fusion* **48** (2006) L1.

4 Tables

	SOLPS5 (kW)	FOIL (kW)	AXUV (kW)
low density D (experiment #32133)			
SOLPS range (simulation #8524)	51.4	58.9	11.9
inside SOLPS		14.4	15.6
outside SOLPS		47.2	9.3
low density He (experiment #32138)			
SOLPS range (simulation #11050)	51.0	59.9	22.61
inside SOLPS		12.2	19.4
outside SOLPS		36.4	14.3
high density D(experiment #30319)			
SOLPS range (simulation #10841)	376	123	27.0
inside SOLPS		40.1	47.3
outside SOLPS		117	32.4
high density He(experiment #30337)			
SOLPS range (simulation #11150)	158	95.8	35.4
inside SOLPS		24.1	27.9
outside SOLPS		76.2	25.0

Table 1. The total radiated power calculated for the three poloidal regions: *SOLPS range* - over the region that corresponds exactly the region covered by SOLPS5 (3 cm inside the midplain separatrix, and 1.8 cm outside of it, then following the flux surfaces), *inside SOLPS* - the region not covered by SOLPS5 inside the separatrix, and *outside SOLPS* - the region not covered by SOLPS5 outside the separatrix.

5 Figure captions

Fig. 1. Responsivity of the AXUV diodes and the lines of sights for bolometer cameras (second figure from left) and AXUV cameras (third figure from left), and the magnetic configuration of our SNL configuration.

Fig. 2. *(a)* The plasma effective charge for low density D discharge (#32133). *(b)* Total radiative powers measured by the foil bolometers (dashed blue line) and AXUV diodes (solid blue line), the power reaching the divertor targets measured by Langmuir probes (black line), the Ohmic input power (green line) and the sum of the foil bolometer power and divertor target power (magenta line).

Fig. 3. *(a)* The plasma effective charge for low density He discharge (#32138). *(b)* Total radiative powers measured by the foil bolometers (dashed blue line) and AXUV diodes (solid blue line), the power reaching the divertor targets measured by Langmuir probes (black line), the Ohmic input power (green line) and the sum of the foil bolometer power and divertor target power (magenta line).

Fig. 4. Total radiative powers for the high density D discharge (#30319) measured by the foil bolometers (dashed blue line) and AXUV diodes (solid blue line), the power reaching the divertor targets measured by Langmuir probes (black line and triangles), the Ohmic input power (green line and squares) and the sum of the foil bolometer power and divertor target power (magenta line and circles).

Fig. 5. Total radiative powers for the high density He discharge (#30337) measured by the foil bolometers (dashed blue line) and AXUV diodes (solid blue line), the power reaching the divertor targets measured by Langmuir probes (black line and triangles), the Ohmic input power (green line and squares) and the sum of the foil bolometer power and divertor target power (magenta line and circles).

Fig. 6. Total radiative power distributions according to a SOLPS5 simulation (a) and according to a tomographic image of foil bolometer signals (b) of a low density D discharge. The numbers correspond to the power emitted by a given poloidal area integrated over its toroidal volume. The area enclosed by the two white lines is covered by the SOLPS5 simulation. Red line – the separatrix

Fig. 7. Same as Fig. 6 but for a low density He discharge.

Fig. 8. Same as Fig. 6 but for a high density De discharge.

Fig. 9. Same as Fig. 6 but for a high density He discharge.

6 Figures

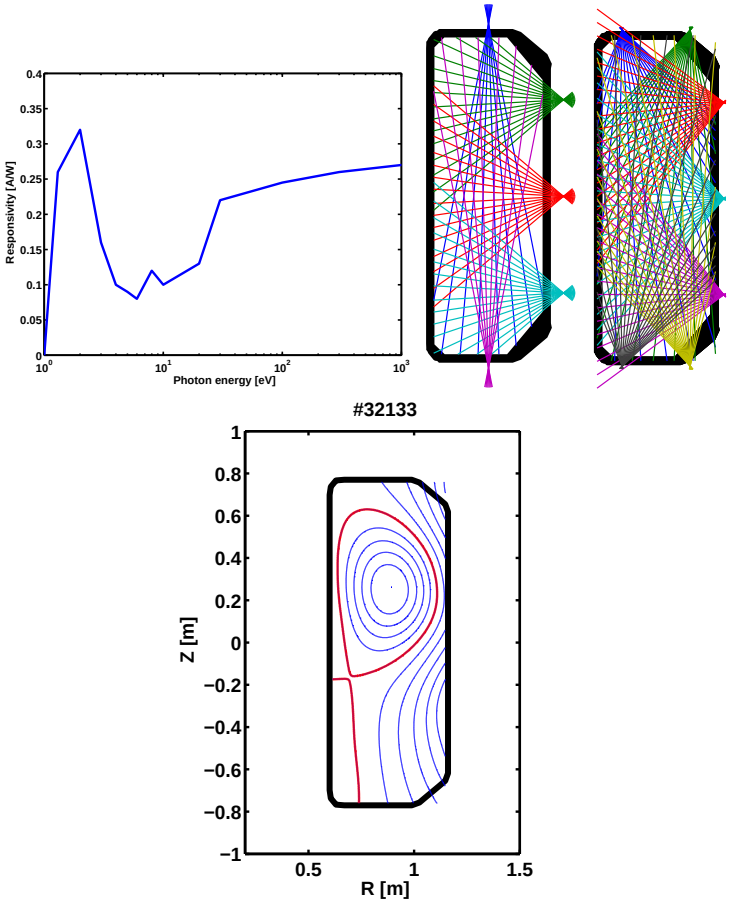

Figure 1

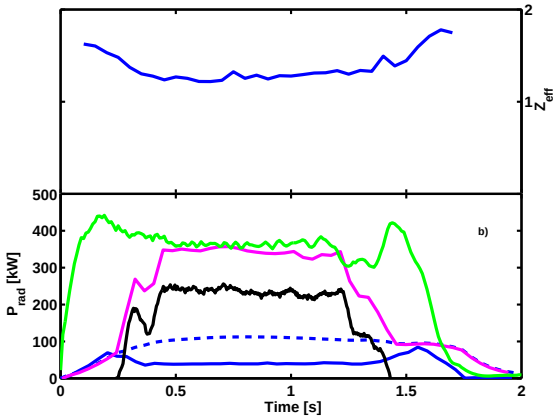

Figure 2

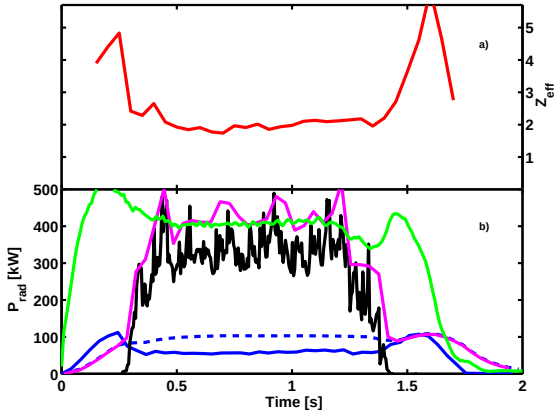

Figure 3

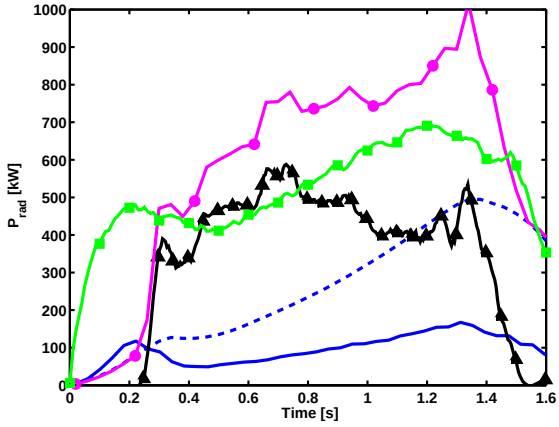

Figure 4

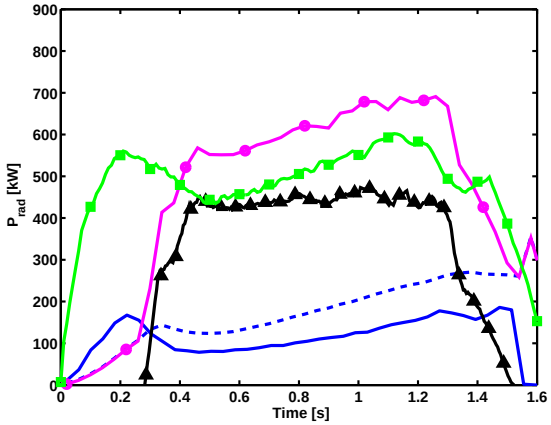

Figure 5

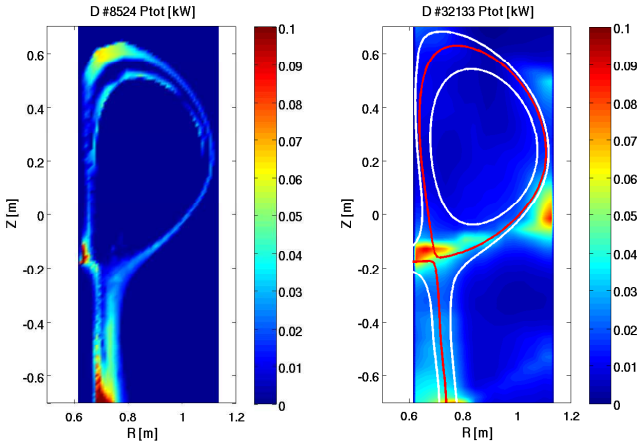

Figure 6

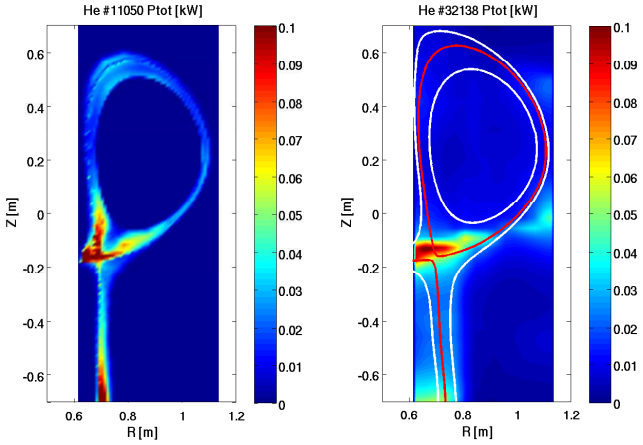

Figure 7

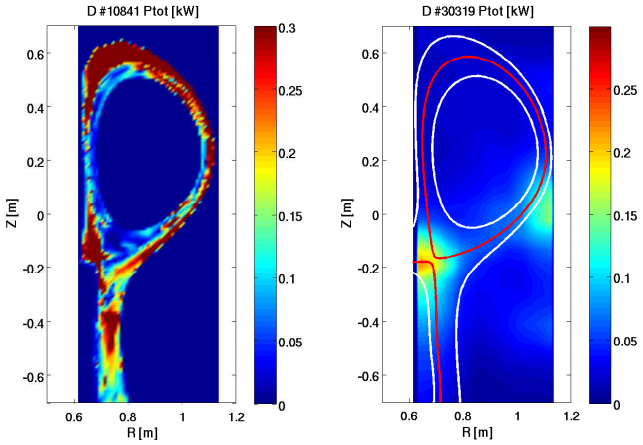

Figure 8

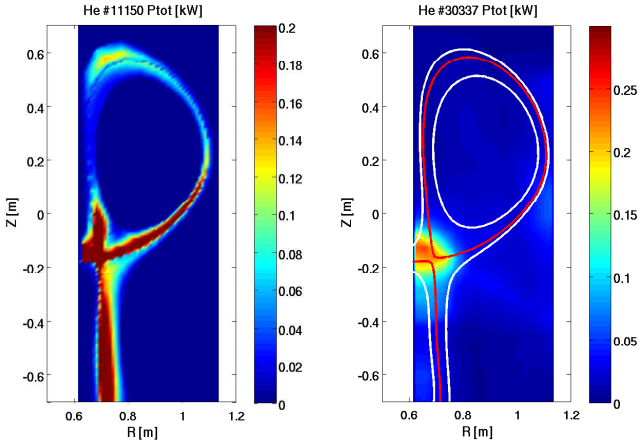
He #11150 Ptot [kW]
He #30337 Ptot [kW]
Z [m]
R [m]
0.6
0.4
0.2
0
-0.2
-0.4
-0.6
0.8
1
1.2
0.2
0.18
0.16
0.14
0.12
0.1
0.08
0.06
0.04
0.02
0
0.25
0.15
0.05

Figure 9